arXiv:2302.03464v1 [cond-mat.mtrl-sci] 7 Feb 2023

Graphical Abstract

Effect of ZrB2 additions on the thermal stability of polycrystalline diamond

Melisha Jivanji, Roy Peter Forbes, Humphrey Sithebe, Johan Ewald Westraadt

Highlights

Effect of ZrB2 additions on the thermal stability of polycrystalline diamond

Melisha Jivanji, Roy Peter Forbes, Humphrey Sithebe, Johan Ewald Westraadt

- ZrB_2 additions converted the catalytic cobalt into non-catalytic Co_2B and $Co_{23}B_6$ phases.
- Onset of bulk graphitisation only occurred at temperatures above 1000 °C for the *ZrB_2-PCD*.
- *ZrB_2-PCD* had excellent thermo-mechanical wear behaviour compared to the standard PCD.

Effect of ZrB2 additions on the thermal stability of polycrystalline diamond

Melisha Jivanji[a,b], Roy Peter Forbes[c], Humphrey Sithebe[b], Johan Ewald Westraadt[a,*]

[a] *Centre for HRTEM, Department of Physics, Nelson Mandela University, Gqeberha, 6031, South Africa*
[b] *Element Six (Pty) Ltd, Springs, 1559, South Africa*
[c] *School of Chemistry, University of the Witwatersrand, Johannesburg, 2000, South Africa*

Abstract

This study investigates the effect of ZrB_2 additions on the microstructure, thermal stability, and thermo-mechanical wear behaviour of polycrystalline diamond. Following high-pressure high-temperature (HPHT) sintering, the *ZrB_2-PCD* material showed a full conversion of the binder phase to cobalt-boride (Co_2B and B_6Co_{23}) phases. In-situ PXRD and TEM vacuum annealing experiments observed that the onset of bulk graphitisation occurred above 1000 °C for the *ZrB_2-PCD* material, compared to 850 °C for the *STD-PCD* material. The *ZrB_2-PCD* tools showed excellent thermo-mechanical wear behaviour, exhibiting increased durability and a steady wear scar progression during high-temperature dry-VTL testing. However, lowered abrasion wear resistance was observed for the *ZrB_2-PCD* tools during low-temperature wet-VTL testing, probably due the reduced diamond contiguity in the ZrB_2 additive sample. Further optimisation of the ZrB_2 additive phase content,

*Please address correspondence to Johan Ewald Westraadt
Email address: johan.westraadt@mandela.ac.za (Johan Ewald Westraadt)

mixing methodology, or sintering conditions could be explored to improve the abrasive wear resistance of this novel PCD material.

Keywords: Polycrystalline diamond, thermal stability, graphitisation, X-ray diffraction, STEM-EELS, vertical turning lathe

1. Introduction

Conventional polycrystalline diamond (PCD) tools are manufactured by sintering diamond powder on a cemented tungsten carbide (WC-Co) substrate, using high pressure (>5.5 GPa) and high temperature (>1450 °C) conditions. During the sintering process, cobalt from the substrate melts and infiltrates into the diamond layer, facilitating the bonding of the diamond grains into a tough, intergrown diamond network. The resulting material has a high micro hardness (50 GPa) and isotropic fracture toughness 8 $MPam^{0.5}$ [1] making it an excellent material in the non-metallic abrasives industries for rock drilling [2], woodworking [3], road-planing, and automotive manufacturing [4].

Despite its superior room temperature properties, PCD materials suffer from thermal instability when exposed to temperatures in excess of 700 °C [5, 6, 7, 8]. The residual metallic binder present in the PCD material following sintering, initiates thermal instability of the tool by inducing graphitisation [5, 7, 8], oxidation [9, 10], and thermal expansion effects [1, 11, 12] at elevated temperatures. These thermally induced degradation mechanisms could lead to premature tool failure and reduced performance.

In this study, thermal stability is defined as the maximum temperature the material can be exposed to before the immediate onset of thermal

degradation. Thermal degradation refers to permanent changes occurring in the material during high temperature exposure, which could include stress-induced cracking, graphitisation, and/or oxidation. There are a variety of methods that can be used to evaluate a materials' thermal stability. The first group of methods involve heat treating the material in a controlled atmosphere and analysing microstructural changes that occur in the material during or after high temperature exposure [13, 10, 8]. This method typically evaluates a specific degradation mechanism (graphitisation, oxidation, or cracking) at controlled temperatures depending on the analysis technique. The second group of methods involve mechanical abrasion testing with a significant thermal component. Increased cutting speeds and/or the absence of a coolant will result in the generation of high temperatures at the tool interface [8]. Since the temperatures at the tool interface are not well controlled, it is usually only used as a ranking tool and the results are usually compared to a suitable benchmark. This method, however, combines all the degradation mechanisms into one test, making it a closer representation of real-world applications. The third method to evaluate thermal stability involves high temperature annealing of the PCD tools in a furnace with a controlled atmosphere and then performing a standard mechanical test thereafter [13, 14]. This method measures the effects of thermal degradation on the mechanical performance of the material. In this study, the thermal stability of the PCD materials were assessed based on its propensity to graphitise during thermal treatments performed under vacuum (method 1) and mechanical abrasion testing using a vertical turning lathe (VTL) with and without a coolant (method 2).

The current industry standard to overcome thermal degradation in PCD materials and prolong the tool life is to remove the metallic cobalt binder phase by acid leaching [15, 16]. Alternatively, ultrahigh pressures and non-metallic binder systems have been used to either minimize or eliminate the metallic binder phase from the PCD material. Akaishi and co-workers [17] used high pressure (7.7 GPa) and temperature (2000 °C) to sinter cobalt-PCD with only 1.5 vol.% metallic binder. Sumiya and co-workers [18] sintered diamond in the absence of a cobalt binder, employing ultrahigh pressure (15 GPa) and temperature (2300 °C) to directly convert graphitic/carbonaceous material into ultrahard nano-polycrystalline diamond. Ceramic binder phases such as TiC [19, 20], TiB_2 [21, 22], and MAX phases [23] have also been used as successful sintering aids for PCD. Sintering of PCD using non-metallic sintering aids has also been demonstrated with carbonates [13, 14, 24]. Although these experimental studies were successful in sintering PCD materials, these novel approaches either resulted in reduced mechanical properties (toughness, hardness or wear resistance), due to a lack of adequate diamond intergrowth, or required elevated sintering conditions (>7.7 & >2000 °C), which significantly increase the costs of tool manufacturing. Consequently, none of these methodologies are currently commercially available in the market.

The present study evaluates the effect of ZrB_2 additives on the thermal stability of standard PCD. The addition of additives to the diamond powder does not require major modifications to the existing tool manufacturing technologies. Thus, there are negligible impacts on the manufacturing costs associated with this approach. The aim of the study is to evaluate the effect of ZrB_2 additions on the thermal stability (onset temperature of graphitisation)

of polycrystalline diamond composites measured using powder X-ray diffraction (PXRD) and advanced electron microscopy. Mechanical VTL testing was then used to determine the effect of ZrB_2 on the abrasion performance of the material at low temperature (with coolant) and high temperature (no coolant) conditions.

2. Methodology

The cylindrical tool (ϕ = 16 mm; height = 12 mm) consisted of a 2 mm thick polycrystalline diamond layer sintered on top of a WC-Co (12 wt%) substrate. Diamond powder (mean particle size: 16 µm) with 10 wt% ZrB_2 additions (*ZrB_2-PCD*) and without (*STD-PCD*) were sintered at $\approx$ 7.0 GPa and 1700 °C in a cubic press system. Figure 1 illustrates the assembly used for synthesis.

Samples 10 mm in diameter and 1 mm thick were removed from the PCD layer using electro-discharge machining for the powder X-ray diffraction (PXRD) analysis. Cross-sectional samples were cut through the diamond layer into the WC-Co substrate and polished to a 1 μm finish using a diamond impregnated resin wheel for the scanning electron microscopy (SEM) analyses. Phase analysis of the as-sintered samples was performed using a Bruker D2 Phaser diffractometer equipped with a Co x-ray source, Lynx eye PSD detector, with pseudo Bragg-Brentano geometry. Polished cross-sections were imaged using backscattered electrons (BSE) in an JEOL7001F SEM (10 keV) equipped with energy dispersive spectroscopy (EDS) capabilities. Image segmentation and quantitative microstructural analyses were performed on the BSE-SEM images using the MIPAR software package [25] in order to deter-

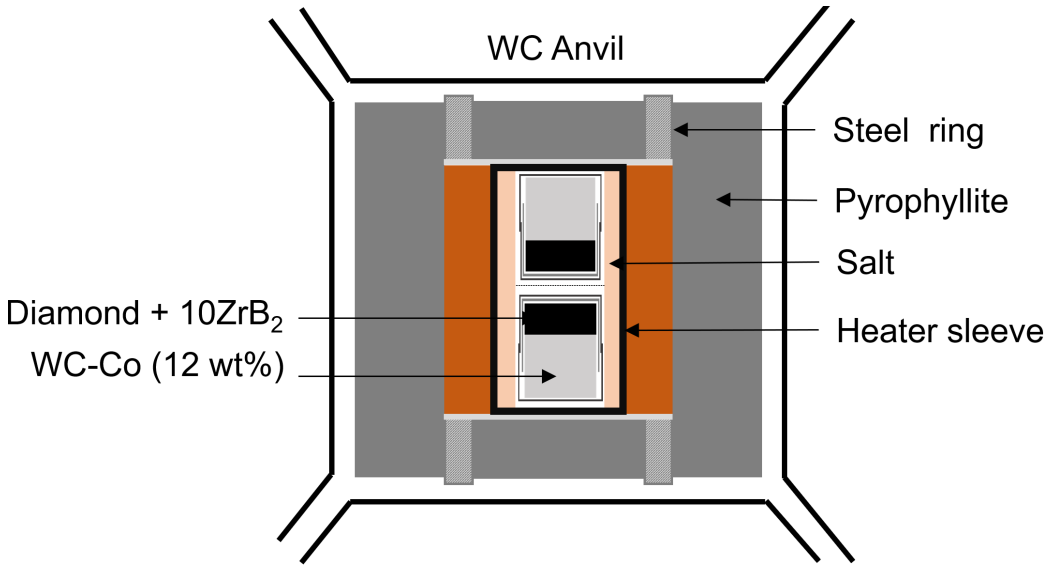


Figure 1: Schematic diagram of the cubic press capsule used for sintering

mine diamond phase fraction, binder phase fraction, diamond grain size, and diamond-phase contiguity [26]. Thin lamellae were removed from the binder phases of the two sintered samples using focused (Ga) ion-beam (FIB)-SEM. The thin sections were then analysed using transmission Kikuchi diffraction (TKD)-EDS in the SEM and selected area electron diffraction (SAED) in the transmission electron microscope to determine the crystal structure of the binder phases. In-situ PXRD data were collected on a PANalytical XPert Pro diffractometer equipped with an Anton Paar HTK1200 reaction chamber ($\lambda_{Co} = 1.789\,\text{Å}$). The non-ambient heating was performed under vacuum, at a pressure of 0.1×10^5 kPa using a stepped profile from 800 °C up to 1100 °C. PXRD patterns were collected every 15 minutes from 15-65 $2\theta°$. The collected PXRD data were processed using Bruker AXS TOPAS (Version 5, 2014) to track the microstructural evolution using the whole pattern fitting approach.

The patterns collected at non-ambient conditions were sequentially refined to track the phase fractions and lattice parameters of the crystallographic phases. A probe corrected JEOL ARM 200F transmission electron microscope operated at 200 kV was used for the analysis in the present study. High angle annular dark field (HAADF) scanning transmission electron microscopy (STEM) imaging sensitive to atomic number variations within the sample, and electron energy loss spectroscopy (EELS) spectrum imaging (SI) were performed using the DualEELS mode on a Gatan GIF Quantum ERS spectrometer. Carbon (diamond and graphite) and cobalt phase maps were extracted by performing multi linear least squares fitting (MLLS) on the 3D data cube after splicing the low-loss and high-loss SIs together. Reference spectra for the background, diamond, graphite, and cobalt phases were extracted from the experimental data set and used in the MLLS analysis. The thin lamellae were mounted on a single-tilt DENSsolutions heating chip. The samples were heated from $450 - 900\,^{\circ}\mathrm{C}$ in intervals of $100\,^{\circ}\mathrm{C}$. The samples were held for 10 minutes at each temperature interval after which imaging was performed using HAADF-STEM. The presence of suspected graphitic phases were confirmed using STEM-EELS analysis, while elemental analysis of carbide phases were done using STEM-EDS.

Mechanical testing was performed using a vertical turning lathe (VTL) testing. The PCD tools were brazed into steel holders and tested on a South African Granite (UCS: 200 MPa) work-piece rotating at 100 RPM. Testing was performed with a water coolant (wet-VTL) and without (dry-VTL), with each test having slightly different testing parameters. The wet-VTL testing conditions prevented excessive heating on the cutting edge, thus measuring

the abrasion resistance of the tool. The tools were tested for 30 passes in the wet-VTL test, thereafter the wear scar area was measured using an optical profilometer. The dry-VTL testing used no coolant, thereby generating more frictional heating at the cutting surface. The dry testing conditions give an indication of the thermo-mechanical wear behaviour of the tools. During dry-VTL testing, the tools were tested at intervals of 2 passes and stopped once the wear scar area progressed into the carbide layer.

3. Results

The PXRD phase analyses performed on the starting states (Figure 2) shows that *ZrB_2-PCD* consisted of diamond, WC, ZrC, Co_2B (ICSD: 5924), and B_6Co_{23} (ICSD: 613389) phases. The cobalt peak (200) observed in *STD-PCD* was not detected in *ZrB_2-PCD*, suggesting that either the cobalt concentration fell below the detection limit of the instrument, or that it was not present as a fcc cobalt phase, but rather as cobalt boride phases (Co_2B and B_6Co_{23}).

The *STD-PCD* microstructure (Figure 3a) consisted of diamond particles (dark phase) surrounded by a cobalt binder phase. WC particles (bright phase) can be seen dispersed within the microstructure. The larger diamond particles show good intergrowth with a fine distribution of cobalt phase around the perimeter of the diamond particles. The *ZrB_2-PCD* sample (Figure 3b) displayed similar microstructural characteristics, but it also contained several larger ($>5\,\mu$m) binder phase regions consisting of a Zr-containing rim and a Co-containing core (Figure 3 coloured EDS map insert).

TKD-EDS crystallographic phase and elemental analysis confirmed that

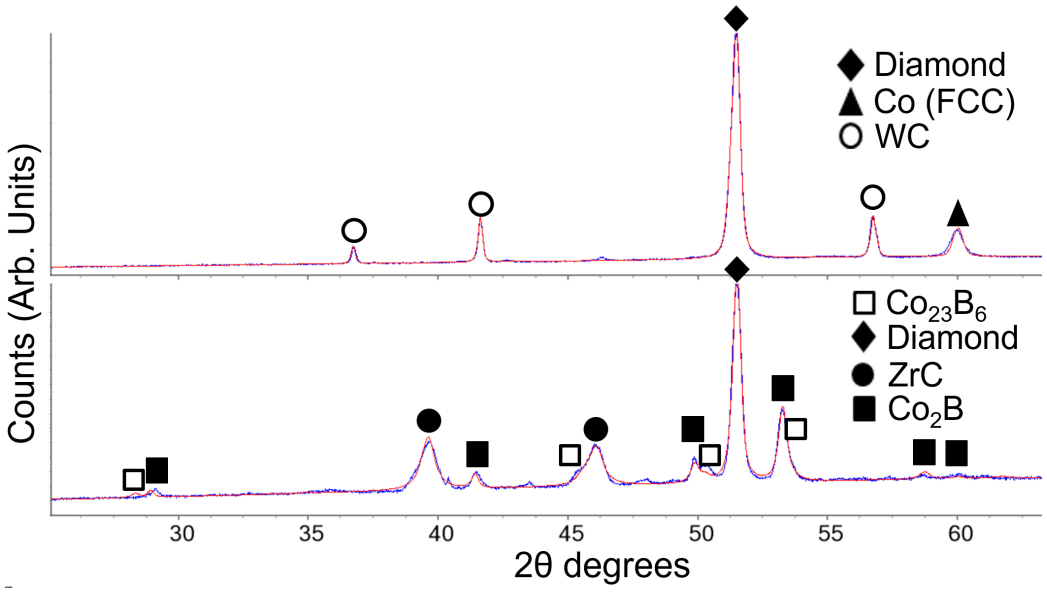


Figure 2: PXRD analysis of the *ZrB_2-PCD* and *STD-PCD* starting states.

the larger binder phase area consisted of a ZrC (rim) and an inner (non-indexed) Co-containing phase (Figure 4). Experimental SAED patterns of this Co-containing phase collected at three different zone axes orientations were successfully matched to the [110], [213], and [112] simulated diffraction patterns of the B_6Co_{23} (ICSD: 613389) phase. This result is in agreement with the bulk PXRD analysis that suggests that boron from the ZrB_2 additions reacted with the infiltrated cobalt metal to form boride (Co_2B and B_6Co_{23}) phases, while the zirconium reacted with carbon to form ZrC particles during sintering.

Quantitative image analysis were performed on BSE images taken at several locations on the polished cross-sectional samples (Table 1). The *ZrB_2-PCD* sample had a lower diamond content (90.3 vol. %) compared to the

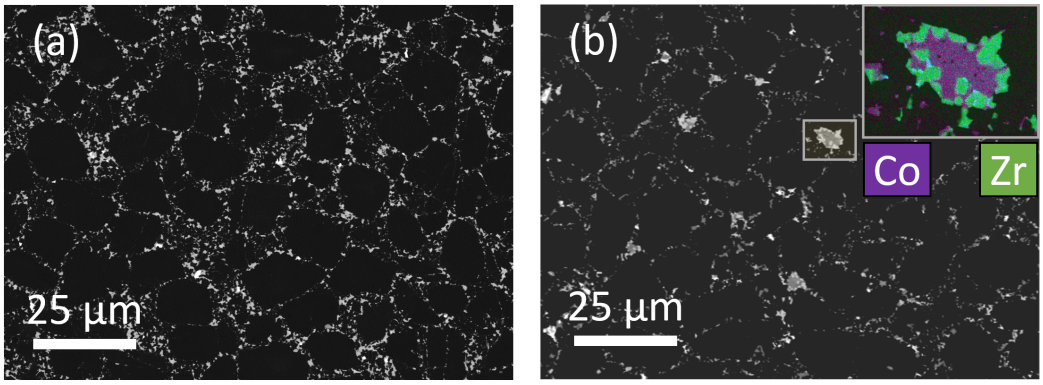


Figure 3: BSE images of (a) *STD-PCD* and (b) *ZrB_2-PCD*. Insert shows an EDS map of the larger ZrC-(CoB_2, B_6Co_{23}) binder pools.

STD-PCD sample due to the presence of an additional 4.5 vol.% ZrC particles in the microstructure. Consequently, the diamond-diamond contact area (contiguity) was also lower (55 %) for the *ZrB_2-PCD* sample due to the presence of this third phase.

Table 1: Quantitative image analysis for the as-sintered samples.

Sample	**Diamond (f_v)**	**Cobalt (f_v)**	**Contiguity (%)**
STD-PCD	93.1 (0.4)	6.9 (0.4)	61 (2)
ZrB_2-PCD	90.2 (0.5)	4.5 (0.1)	55 (4)

3.1. In-situ annealing of polycrystalline diamond

The topographical view of the non-ambient PXRD analysis of the *STD-PCD* and *ZrB_2-PCD* samples are shown in Figure 5. The *STD-PCD* showed a decrease in the cobalt lattice parameter accompanied by the formation of Co_3W_3C η-phase for temperatures between 800 - 850 °C, which is consistent

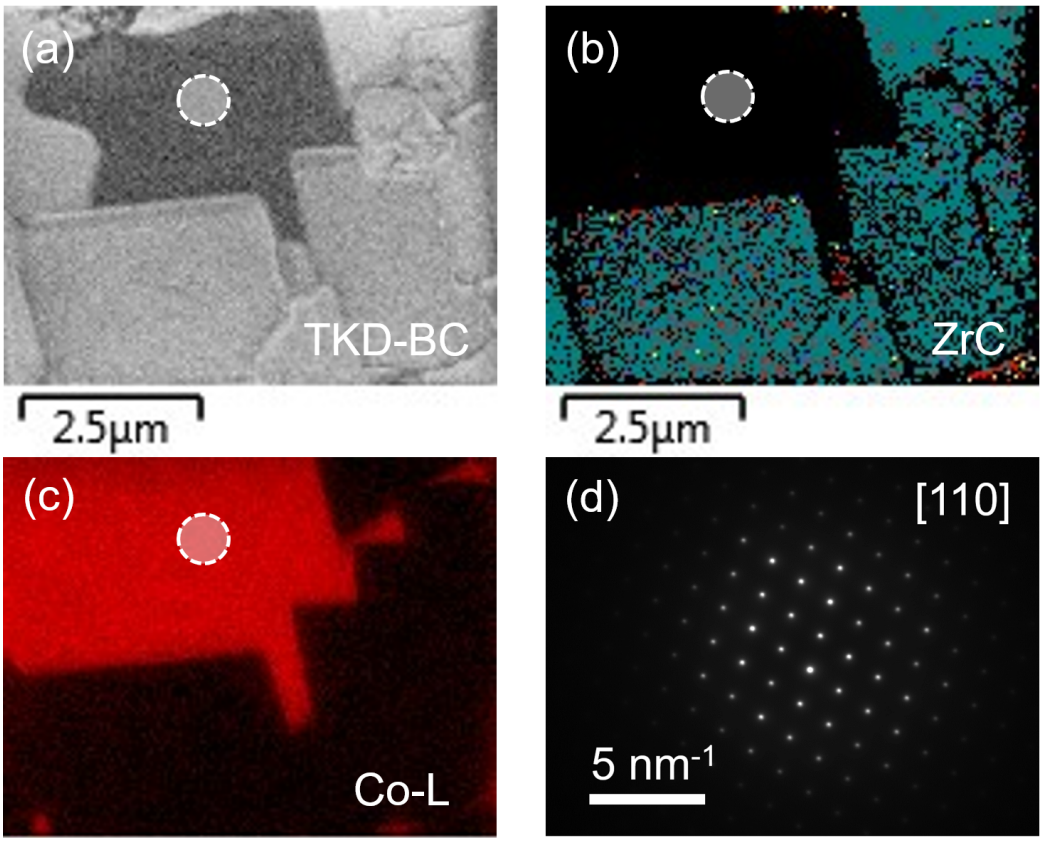


Figure 4: TKD-EDS analysis of the large binder phase particle showing (a) band contrast, (b) phase map, (c) Co-L EDX map, and (d) B=110 SAED the of B_6Co_{23} phase.

with previous high-temperature annealing studies of PCD [8, 27]. According to the PXRD data, graphite was first observed at 850 °C in the *STD-PCD* sample. Quantitative phase analysis of graphite for the *STD-PCD* sample (Figure 6) shows a rapid increase of the graphite phase fraction at 850 °C, which then plateaued at approximately 7 wt%. There were several additional microstructural changes that occurred in the *STD-PCD* sample during high-temperature annealing in vacuum, but this will be the subject of future study.

In contrast, the *ZrB_2-PCD* sample showed no observable microstructural changes during vacuum annealing at 800 - 1000 °C. According to the PXRD data,graphite was first observed after 1000 °C in the *ZrB_2-PCD* sample. The peak heights of the Co_2B phase decreased after 1000 °C heat treatment. Quantitative phase analysis of graphite for the *ZrB_2-PCD* sample (Figure 6) showed a gradual increase, which remained below 2 wt% up until 1100 °C. The decrease in the Co_2B phase fraction could not be accurately quantified due to its low relative abundance in the presence of other highly crystalline phases as well as a loss in the quality of the data which is affected by additional scattering effects brought about at elevated temperatures. Therefore, the possible decomposition of the boride phases into a pure cobalt phase could not be confirmed from this particular PXRD data set.

HAADF-STEM images of the samples after in-situ TEM annealing for 10 minutes at 700 °C, 800 °C, and 900 °C are shown in Figure 7. The samples were evaluated for suspected graphite using image contrast which was then confirmed using STEM-EELS analysis, indicated by red arrows on the HAADF-STEM images. No graphite formation was observed for annealing temperatures up to 700 °C. The onset of graphite formation occurred within

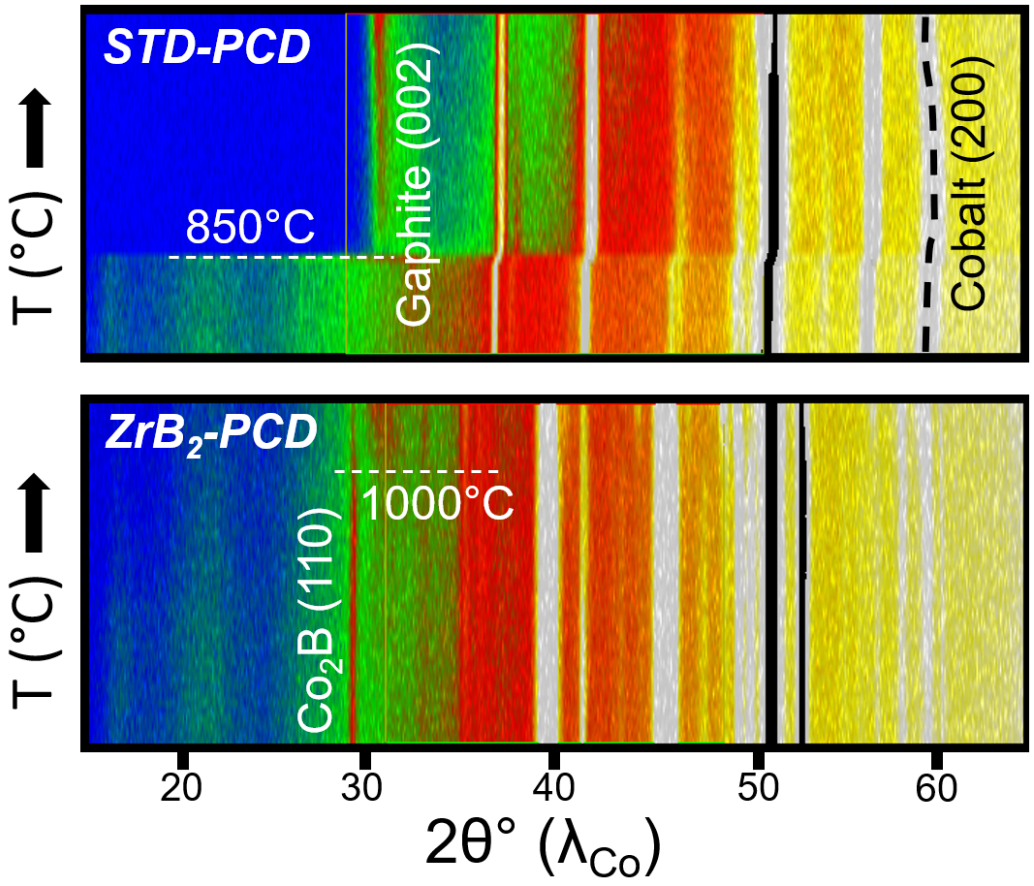


Figure 5: Topographical plot of the in-situ PXRD intensity showing the microstructural changes that occurred in the samples during high temperature annealing in vacuum.

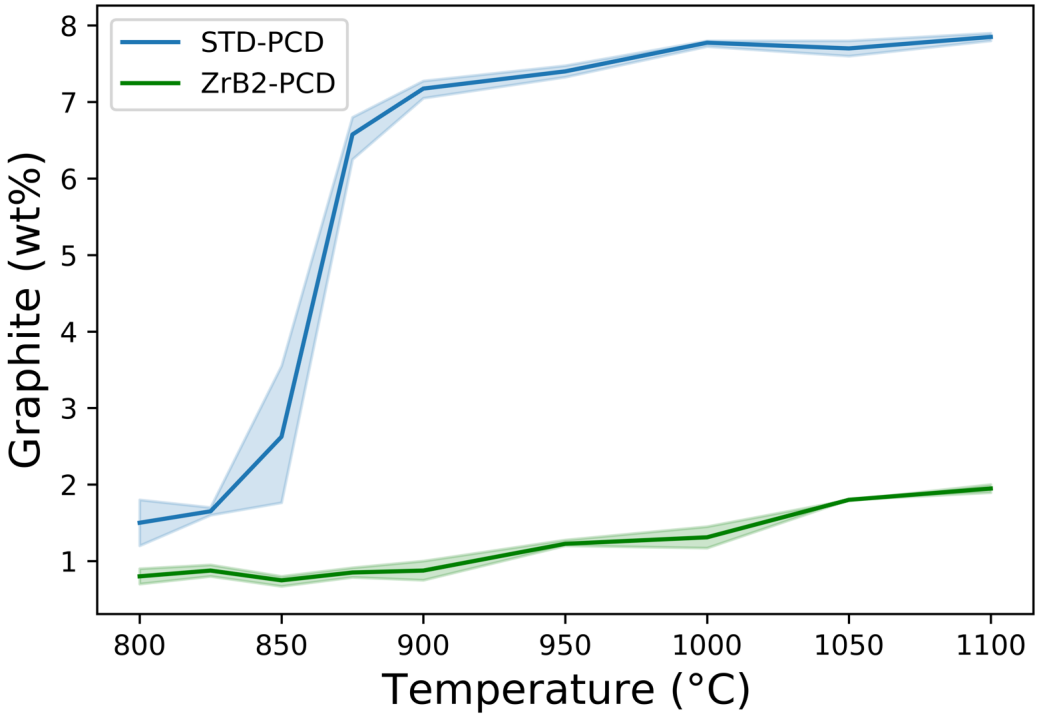


Figure 6: Quantitative phase analysis obtained from the PXRD data for graphite in the vacuum annealed samples.

10 minutes of heating at 800 °C for the *STD-PCD* sample, with multiple graphitic carbon sites confirmed at the cobalt/diamond interface. Graphite formation continued rapidly in the *STD-PCD* sample as the temperature was increased to 900 °C, extending into the cobalt binder pool. Figure 8 shows a higher magnification HAADF-STEM image and a coloured phase map insert of the cobalt-diamond interface after 800 °C annealing, thus confirming the presence of graphitic carbon. In comparison, HAADF-STEM imaging of the in-situ TEM annealed *ZrB_2-PCD* sample showed only minor signs of graphite formation after 10 minutes of heating at 800 °C. Subsequent annealing at 900 °C for 10 minutes, showed no additional graphitic nucleation sites and no appreciable growth of the existing graphite sites.

3.2. Thermo-mechanical VTL testing

Vertical turning lathe (VTL) testing were performed to investigate the thermo-mechanical wear behaviour of the polycrystalline diamond materials sintered with ZrB_2 additions. The dry-VTL testing results are shown in Figure 9. The *STD-PCD* sample tools (n=2) (*STD-PCD (NL)*) failed after the first set of 10 passes after developing a large wear scar that extended into the WC-Co substrate. *STD-PCD* tools (n=3) leached to a depth of 250 μm (*STD-PCD (L)*) showed initial wear scar progressions similar to the *ZrB_2-PCD* samples, but failed catastrophically after 30-32 passes. The *ZrB_2-PCD* tools (n=3) had a steady wear scar progression until 75, 104, and 120 passes, when the wear scars reached the WC-Co substrate and the testing was stopped.

Following the dry-VTL testing, SEM analysis of the wear scar area was performed in order to investigate the failure mechanisms for both materials.

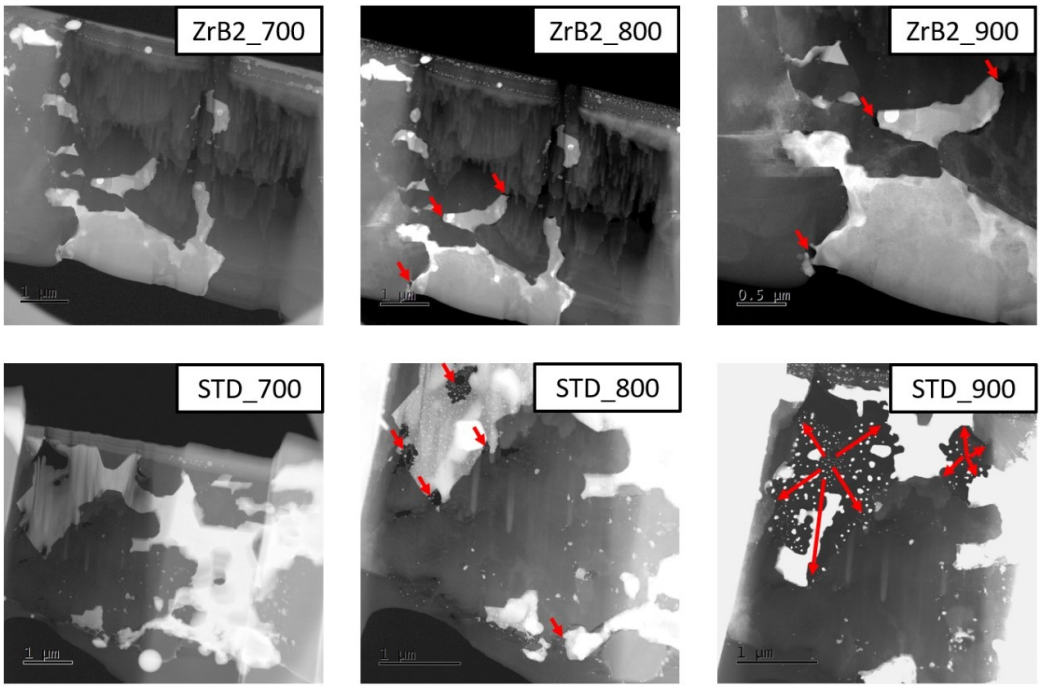


Figure 7: HAADF-STEM images of the *ZrB_2-PCD* (top) and *STD-PCD* (bottom) samples after 10 minutes of in-situ TEM annealing at the various temperatures. The confirmed presence of graphitic carbon is indicated with red arrows.

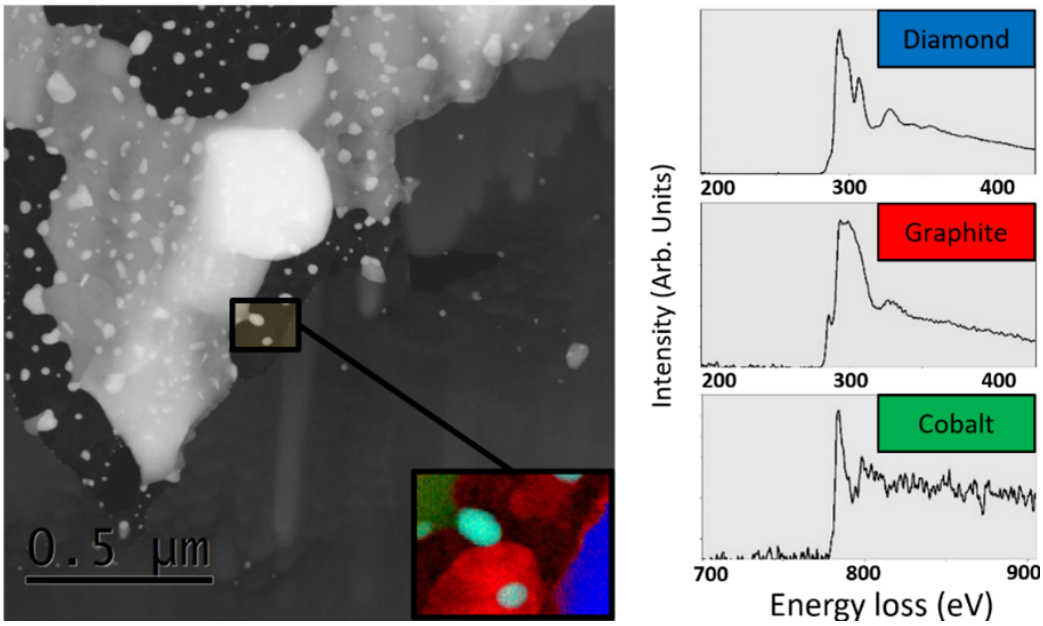


Figure 8: HAADF-STEM image of a Co-W binder pool after in-situ TEM annealing at 850 °C for 10 minutes. The insert shows a STEM-EELS coloured phase map of the binder/diamond interface, indicating the distribution of diamond (blue), graphite (red) and cobalt (green). The corresponding electron energy loss spectra used in the MLLS fitting are shown on the right.

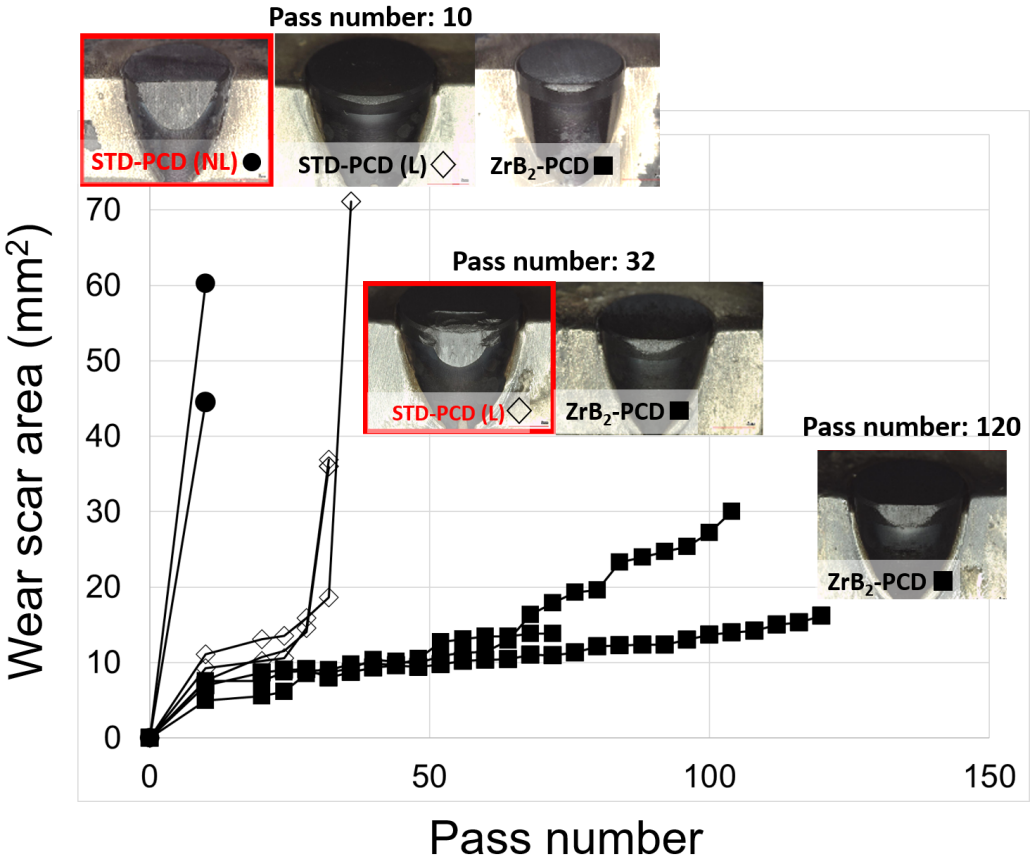


Figure 9: Thermo-mechanical wear testing of the samples using the dry-VTL testing conditions. (**NL**: non-leached; **L**: 250 μm acid leach)

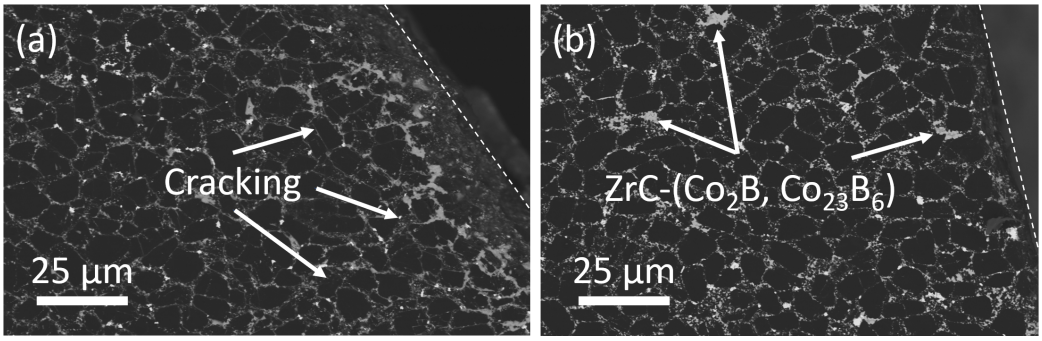


Figure 10: BSE-SEM images of the wear scar area for (a) *STD-PCD* and (b) *ZrB_2-PCD* following the dry-VTL testing.

Figure 10 shows the BSE-SEM images of the tools cross-sectioned through the wear scar area indicated by the dashed line. The *STD-PCD* sample showed a compromised diamond structure with transgranular cracks and several large SiO_2 inclusions (confirmed with EDS analysis - not shown). The origin on the SiO_2 inclusions is probably due to contaminants from the polishing wheel being deposited into larger cavities created during the high-temperature wear test. The premature failure of the tool (10 passes) was due to thermal degradation for the unleached *STD-PCD* sample.

The *ZrB_2-PCD* wear scar did not show extensive transgranular cracking observed in the *STD-PCD* sample and there were no SiO_2 inclusions embedded during the polishing process. This indicates that the integrity of the diamond structure was maintained through the duration of the high-temperature wear test. There were no evidence for thermal degradation in the *ZrB_2-PCD* sample from the SEM analysis, which confirms that the ZrB_2 additions improved the thermal stability of the PCD tool.

The truncated wet-VTL testing generate lower temperatures at the tool

interface and is a measure of the tools' ability to withstand abrasive wear. The mechanical properties in PCD materials are related to the diamond-diamond contact area (Contiguity %) and the strength of the diamond-diamond intergrown structure. The *ZrB_2-PCD* tools (n=4) showed a larger wear scar (17.2 ± 0.3 mm^2) compared to the *STD-PCD* (10.1 ± 0.4 mm^2) tools (n=4) for the wet-VTL testing truncated to 30 passes. This result implies the abrasion wear of the PCD tools was reduced by the addition of ZrB_2 to the diamond powder.

4. Discussion

4.1. Effect on the as-sintered microstructure

The addition of ZrB_2 to the diamond powder prior to sintering resulted in an intergrown diamond microstructure containing residual cobalt-boride (Co_2B, $Co_{23}B_6$) phases. Larger binder areas consisting of a ZrC outer rim and an cobalt-boride inner core are distributed throughout the microstructure (Figure 3 and Figure 10). The ZrB_2 phase reacted with the molten cobalt during sintering to form the cobalt-boride and ZrC phases. The diamond phase fraction (f_v) and diamond phase contiguity (%) of the *ZrB_2-PCD* was lower than the *STD-PCD* material due to the formation of a ZrC secondary phase. PXRD analysis could not detect a pure cobalt phase in the *ZrB_2-PCD* sample and all the cobalt were converted into cobalt-boride phases.

4.2. Effect on the catalytic graphitisation

Metal-boride interlayers are commonly used to prevent catalytic graphitisation of diamond coatings grown on WC-Co and steel cutting tools [28, 29].

Thus the catalytic conversion of diamond to graphite for the cobalt-boride binder was expected to be lower relative to the pure cobalt binder phase present in the *STD-PCD* sample. The *ZrB_2-PCD* sample only showed measurable bulk graphitisation at temperatures above 1000 °C, compared to the *STD-PCD* sample that graphitised at 850 °C during the in-situ PXRD analysis. During in-situ TEM annealing, STEM-EELS analysis showed that graphite was first observed at 800 °C for both samples, but the subsequent graphite growth was more pronounced for the *STD-PCD* sample at 900 °C. This shows that the ZrB_2 additives resulted in a more thermally stable (Co_2B and B_6Co_{23}) binder phase with a lower propensity for diamond-to-graphite conversion during elevated temperature annealing performed in vacuum.

4.3. Effect on the thermo-mechanical wear properties

The *ZrB_2-PCD* sample showed a significant improvement in the high temperature dry-VTL testing as compared to the *STD-PCD*. The high temperatures generated at the cutting interface resulted in transgranular cracking and cavity formation, which resulted in early failure of the unleached *STD-PCD* tools after just 10 passes. The thermally degraded microstructure of the *STD-PCD* tool was similar to that of a previous study on high temperature milling of granite using a similar PCD tool [8]. The leached (250 μm depth) *STD-PCD* sample showed a wear scar progression similar to the *ZrB_2-PCD* sample for the initial stages, but then rapidly degraded and failed catastrophically after 32 passes. In contrast the *ZrB_2-PCD* sample showed no obvious microstructural evidence of thermal degradation and exhibited a controlled wear scar progression into the WC-Co substrate after 120 passes.

The abrasive wear properties and hardness of PCD tools are directly related to the intergrown diamond network, where a higher phase fraction of diamond have been linked to an increased hardness and "grinding resistance" for PCD materials sintered with less binder phase at elevated pressures [17]. Ultrahard ceramic materials such as PCD have an inherently low fracture toughness ($8\,\mathrm{MPam}^{0.5}$), which is then further negatively affected by microstructural flaws [30]. PCD materials containing poorly bonded diamond-diamond particles, large inclusions, or cavities post-sintering would negatively affect the fracture behaviour of the tool during abrasive testing. The *ZrB_2-PCD* sample had a larger wear scar compared to the *STD-PCD* sample in the truncated wet-VTL test. The reduced abrasive wear resistance of *ZrB_2-PCD* sample could be due to the larger binder pools with ZrC inclusions, which resulted lower diamond phase fraction, reduced diamond-diamond intergrowth, and could also have acted as microstructural flaws negatively affecting the fracture behaviour of the tool. In addition, boron could have influenced the ability of cobalt to act as an effective sintering aid for diamond intergrowth.

Since the primary advantage of PCD tools in application is its high abrasion resistance, it is imperative that its inherent mechanical performance should not be compromised by the additive. The VTL testing data highlights an important trade-off that exist when evaluating new thermally stable PCD materials based on binder additives. This study demonstrate the intimate link between processing-microstructure-properties, and highlights the importance of tailoring the processing and/or microstructure to achieve the desired balance between abrasive wear resistance and thermal stability.

In order to improve the abrasion resistance of the *ZrB_2-PCD* material, while still retaining its exceptional thermal stability a number of optimisations can be explored. A reduction in the particle size and phase fraction of the residual ZrC phase is required. This could be achieved via better control of the starting particle size, additive content, or more homogeneous mixing of the ZrB_2 additives. Furthermore, increasing the sintering conditions using higher pressure and/or higher temperature could potentially offset the negative effects that boron could have on the cobalt to act as a liquid phase sintering aid.

5. Conclusions

From the characterisation data presented and discussed here we can draw the following conclusions about the materials:

- The addition of 10 wt% ZrB_2 to the diamond powder prior to sintering yielded an intergrown diamond structure with a complete conversion of the residual binder to cobalt-boride (Co_2B, $Co_{23}B_6$) phases.
- The onset of bulk graphitisation in the *ZrB_2-PCD* material was improved to temperatures above 1000 °C compared to the 850 °C onset observed for the *STD-PCD* material.
- The *ZrB_2-PCD* tool had excellent thermo-mechanical wear performance in dry-VTL testing and the microstructure showed no evidence of thermal degradation.
- However, the abrasion wear performance of the *ZrB_2-PCD* tool in wet-VTL testing was compromised, due to the presence of 4.5 vol.% ZrC

phase, resulting in reduced diamond-diamond intergrowth (diamond f_v and contiguity %).

Data availability

The raw data required to reproduce these finding are available to download after a request to the corresponding author.

Declaration of Competing Interest

The authors declare that they have no known competing financial interests or personal relationships that could have appeared to influence the work reported in this paper.

Acknowledgement

JEW and MJ gratefully acknowledge financial support of the National Research Foundation of South Africa (Grant number 70724). We also acknowledge the assistance of Mohsen Danaie and Christopher S. Allen from the electron Physical Science Imaging Centre (ePSIC) at the Diamond Light Source (Ltd) with the collection of the in-situ TEM data (Instrument E01, proposal MG26338) and David Aldmington from the Global Innovation Centre (GIC) at Element Six (Pty) Ltd with the collection of the in-situ PXRD data.

References

[1] M. W. Cook, P. K. Bossom, Trends and recent developments in the material manufacture and cutting tool application of polycrystalline diamond and polycrystalline cubic boron nitride, International Journal of Refractory Metals and Hard Materials 18 (2) (2000) 147–152. doi:10.1016/S0263-4368(00)00015-9.

[2] D. E. Scott, The history and impact of synthetic diamond cutters and diamond enhanced inserts on the oil and gas industry, Industrial Diamond Review (2006) 48–55.

[3] P. Philbin, S. Gordon, Characterisation of the wear behaviour of polycrystalline diamond (PCD) tools when machining wood-based composites, Journal of Materials Processing Technology 162–163 (2005) 665–672. doi:10.1016/j.jmatprotec.2005.02.085.

[4] V. P. Astakhov, A. Stanley, Polycrystalline Diamond (PCD) Tool Material: Emerging Applications, Problems, and Possible Solutions, in: J. P. Davim (Ed.), Traditional Machining Processes: Research Advances, Materials Forming, Machining and Tribology, Springer, Berlin, Heidelberg, 2015, pp. 1–32. doi:10.1007/978-3-662-45088-8_1.

[5] R. L. Mehan, L. E. Hibbs, Thermal degradation of sintered diamond compacts, Journal of Materials Science 24 (3) (1989) 942–950. doi:10.1007/BF01148782.

[6] M. V. Sneddon, D. R. Hall, Recent Advances in Polycrystalline Diamond (PCD) Technology Open New Frontiers in Drilling, in: SPE Annual Technical Conference and Exhibition, OnePetro, 1987. doi:10.2118/17007-MS.

[7] L. Tze-Pin, M. Hood, G. A. Cooper, L. Xiaohong, Wear and failure mechanisms of polycrystalline diamond compact bits, Wear 156 (1) (1992) 133–150. doi:10.1016/0043-1648(92)90149-3.

[8] J. E. Westraadt, I. Sigalas, J. H. Neethling, Characterisation of thermally degraded polycrystalline diamond, International Journal of Refractory Metals and Hard Materials 48 (2015) 286–292. doi:10.1016/j.ijrmhm.2014.08.008.

[9] T. Evans, C. Phaal, The Kinetics of the Diamond-Oxygen Reaction, in: Proceedings of the Fifth Conference on Carbon, Pergamon, 1962, pp. 147–153. doi:10.1016/B978-0-08-009707-7.50025-X.

[10] D. Miess, G. Rai, Fracture toughness and thermal resistance of polycrystalline diamond compacts, Materials Science and Engineering: A 209 (1) (1996) 270–276. doi:10.1016/0921-5093(95)10105-5.

[11] J. Gu, K. Huang, Role of cobalt of polycrystalline diamond compact (PDC) in drilling process, Diamond and Related Materials 66 (2016) 98–101. doi:10.1016/j.diamond.2016.03.025.

[12] S. Shimada, H. Tanaka, M. Higuchi, T. Yamaguchi, S. Honda, K. Obata, Thermo-Chemical Wear Mechanism of Diamond Tool in Machining of Ferrous Metals, CIRP Annals 53 (1) (2004) 57–60. doi:10.1016/S0007-8506(07)60644-1.

[13] M. Akaishi, S. Yamaoka, F. Ueda, T. Ohashi, Synthesis of polycrystalline diamond compact with magnesium carbonate and its physical properties, Diamond and Related Materials 5 (1) (1996) 2–7. doi:10.1016/0925-9635(95)00332-0.

[14] J. E. Westraadt, N. Dubrovinskaia, J. H. Neethling, I. Sigalas, Thermally stable polycrystalline diamond sintered with calcium carbon-

ate, Diamond and Related Materials 16 (11) (2007) 1929–1935. doi:10.1016/j.diamond.2007.08.011.

[15] H. P. Bovenkerk, P. D. Gigl, Temperature resistant abrasive compact and method for making same (Sep. 1981).

[16] N. Griffin, P. Hughes, High volume density polycrystalline diamond with working surfaces depleted of catalyzing material (Mar. 2002).

[17] M. Akaishi, S. Yamaoka, J. Tanaka, T. Ohsawa, O. Fukunaga, Synthesis of sintered diamond with a high electrical resitivity and high hardness, Materials Science and Engineering: A 105–106 (1988) 517–523. doi:10.1016/0025-5416(88)90738-0.

[18] H. Sumiya, T. Irifune, A. Kurio, S. Sakamoto, T. Inoue, Microstructure features of polycrystalline diamond synthesized directly from graphite under static high pressure, Journal of Materials Science 39 (2) (2004) 445–450. doi:10.1023/B:JMSC.0000011496.15996.44.

[19] V. M. das Chagas, M. P. Peçanha, R. d. S. Guimarães, A. A. A. dos Santos, M. G. de Azevedo, M. Filgueira, The influence of titanium carbide (TiC) coating over the thermal damage processes in diamonds, Journal of Alloys and Compounds 791 (2019) 438–444. doi:10.1016/j.jallcom.2019.03.285.

[20] S.-M. Hong, M. Akaishi, S. Yamaoka, High-Pressure Synthesis of Heat-Resistant Diamond Composite Using a Diamond-TiC0.6 Powder Mixture, Journal of the American Ceramic Society 82 (9) (1999) 2497–2501. doi:10.1111/j.1151-2916.1999.tb02109.x.

[21] L. Jaworska, P. Klimczyk, M. Szutkowska, P. Putyra, M. Sitarz, S. Cygan, P. Rutkowski, Thermal resistance of PCD materials with borides bonding phase, Journal of Superhard Materials 37 (3) (2015) 155–165. doi:10.3103/S1063457615030028.

[22] X. Sha, W. Yue, H. Zhang, W. Qin, D. She, C. Wang, Thermal stability of polycrystalline diamond compact sintered with boron-coated diamond particles, Diamond and Related Materials 104 (2020). doi:10.1016/j.diamond.2020.107753.

[23] L. Jaworska, M. Szutkowska, J. Morgiel, L. Stobierski, J. Lis, Ti3SiC2 as a bonding phase in diamond composites, Journal of Materials Science Letters 20 (19) (2001) 1783–1786. doi:10.1023/A:1012535100330.

[24] J. Qian, C. E. McMurray, D. K. Mukhopadhyay, J. K. Wiggins, M. A. Vail, K. E. Bertagnolli, Polycrystalline diamond cutters sintered with magnesium carbonate in cubic anvil press, International Journal of Refractory Metals and Hard Materials 31 (2012) 71–75. doi:10.1016/j.ijrmhm.2011.09.008.

[25] J. M. Sosa, D. E. Huber, B. Welk, H. L. Fraser, Development and application of MIPAR™: A novel software package for two- and three-dimensional microstructural characterization, Integrating Materials and Manufacturing Innovation 3 (1) (2014) 123–140. doi:10.1186/2193-9772-3-10.

[26] R. M. German, The contiguity of liquid phase sintered microstructures,

Metallurgical Transactions A 16 (7) (1985) 1247–1252. doi:10.1007/BF02670329.

[27] T. Scott, The effect of high temperature on polycrystalline diamond, Ph.D. thesis, University of Oxford (2019).

[28] W. Tang, Q. Wang, S. Wang, F. Lu, A comparison in performance of diamond coated cemented carbide cutting tools with and without a boride interlayer, Surface and Coatings Technology 153 (2-3) (2002) 298–303. doi:10.1016/S0257-8972(01)01694-2.

[29] D. Damm, A. Contin, F. Barbieri, V. Trava-Airoldi, D. Barquete, E. Corat, Interlayers Applied to CVD Diamond Deposition on Steel Substrate: A Review, Coatings 7 (9) (2017) 141. doi:10.3390/coatings7090141.

[30] T. A. Scott, The influence of microstructure on the mechanical properties of polycrystalline diamond: A literature review, Advances in Applied Ceramics 117 (3) (2017) 161–176. doi:10.1080/17436753.2017.1389462.